# Development, Modeling, and Testing of a Passive Compliant Bistable Undulatory Robot

Anson Kwan<sup>1</sup> and Daniel Aukes<sup>2</sup>

<sup>1</sup> Ira A. Fulton School of Engineering, Arizona State University, Mesa, AZ 85212, USA
<sup>2</sup> School of Manufacturing Systems and Networks, Arizona State University, Mesa, AZ 85212, USA
USA
akwan2@asu.edu

Abstract. This proposed device uses a single actuator to transition a bistable constrained compliant beam to generate undulatory motion. Undulatory locomotion is a unique form of swimming that generates thrust through the propagation of a wave through a fish's body. This paper draws inspiration from Anguilliformes and discusses the kinematics and dynamics of wave propagation of a bistable underwater robot. Thrust generation is explored through modeling and experimentation of the length constraint to better understand the device. This paper validates the theoretical spine behavior through experimentation and provides a path forward for future development in device optimization for various applications. Previous work developed devices that utilized either paired soft actuators or multiple redundant classical actuators that resulted in a complex prototype with intricate controls. Our work contrasts with prior work in that it aims to achieve undulatory motion through passive actuation from a single actively driven point which simplifies the control. Through this work, the goal is to further explore low-cost soft robotics via bistable mechanisms, continuum material properties, and simplified modeling practices.

**Keywords:** Bistable Mechanism, Compliant Material, Anguilliform, Simulation, Bioinspired.

## 1 Introduction

This paper presents a novel, passive, and compliant material system that uses a single actuator accompanied by a rigid length constraint to generate motion inspired by eels. The motivation of our paper is to explore how bistable devices (see Fig. 1) can generate complex motion from simple input signals via careful selection of material properties, beam geometry, and geometric constraints. From this, exploring undulatory swimming is a natural progression, due to its elegant wave propagation dynamics [1]. Our proposed device utilizes the tuned dynamics of a compliant material arranged in a bistable configuration so that when engaged it forces the material to transition between stable states. This generates a wave that propagates along its length, facilitating a swimming gait reminiscent of anguilliform swimmers (see Fig. 2). A pseudo rigid body (PRB) approximation of a flexible material is used to provide a framework for

device optimization and design. The model is validated against an experimental prototype to ensure an accurate analytical model is used for future optimization.

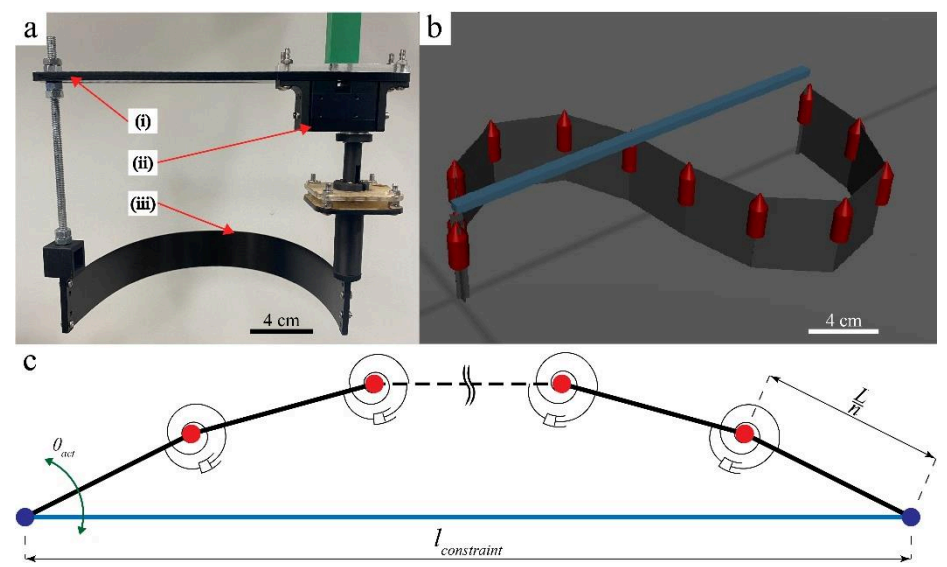


Fig. 1. (a) Manufactured prototype of proposed design comprised of the (i) length constraint mechanism, (ii) Dynamixel Servo, and (iii) fiberglass beam. (b) Orthonormal view of ten-link (gray) PRB connected by hinge joints (red dot). The model was designed so that each link was one tenth of the overall length of the spine and connected to the length constraint (blue). (c) Pseudo-rigid body of n-link (black line) approximation of compliant material. Each joint has a single degree of freedom with a torsional spring (spiral) and rotational damper (dashpot). The length constraint (blue) was then derived as a rigid body that connected each end of the spine by a zero-friction pin joint (blue dot). The angle  $\vartheta_{act}$  of the head drives the position and state of the device (green arrow).

Eels and other body caudal fin (BCF) fish demonstrate 'pure' anguilliform locomotion by way of lateral compression; the compression and release of muscular forces propagate a wave down their spine, which travels along their flexible bodies to create thrust [2][3]. Undulatory locomotion demonstrates outstanding hydromechanical efficiency by generating substantial amounts of momentum via the timed storage and release of energy [2][4]. The release of potential energy through a wave to generate momentum by pushing against water has also inspired roboticists to explore and develop undulatory devices [4]. In the past decade, research has focused on bio-inspired, undulatory swimmers, utilizing both soft bodies and classical rigid mechanics to understand this hydrodynamic effect [4-7]. For these devices, the timing of actuators mounted in series along the body not only limits the adaptability of many prototypes but impedes our ability to mimic nature. In recent years, the push towards simplified robots which utilize soft or compliant materials has enabled new developments in bioinspired swimming devices, which take advantage of material properties, curvature, and asymmetric system stiffness [8-12]. Previous bistable undulatory devices focused on snap-through buckling effects to generate momentum [13]

In contrast with the work above, we propose using geometric constraints alongside bending, compliant beams to create a bistable, dynamic system to develop undulatory locomotion. This study fits under the umbrella of a new class of devices we call "Soft, Curved, Reconfigurable, Anisotropic Mechanisms" (SCRAMs), which we have previously studied in the context of buckling beams [10], pinched tubes [11], and twisted beams [12]. The novelty of this device is highlighted by its simple control, high degree of tunability, and continuous beam deformation due to continuum material and fluidic interaction. A prototype of our device has been simulated and validated experimentally. The model employed is based on a rigid-body approximation of a flexible material; it utilizes estimated environmental forces to help understand locomotion performance in water. The prototype and experimental results both validate the parameterization of the physics-based model and demonstrate several design variables that play a key role in influencing performance.

The rest of this paper is laid out in the following order. In the second section, we describe the approach and methodology of how the proposed device was modeled and experimentally validated. The third section discusses the experimental results and analysis. The fourth section outlines our conclusions on the research and impacts of this concept for future work.

## 2 Approach and Methodology

The following sections outline our intent and procedure for modeling, prototyping, and simulation of the proposed device.

#### 2.1 Analytical Model

The proposed model is shown in Fig. 1. At the top half of the frame, we see a continuum material whose length is constrained by a rigid element of length 'l<sub>constraint</sub>' (see Fig. 1). The approximated pseudo-rigid-body (PRB) model is shown in Fig. 1c with n rigid links connected by a series of hinge joints (shown in red). Other methods of modeling flexible materials utilize shell theory or fabric mechanics, which can generate higher fidelity results, but must often make compromises with the fluidic models to balance computational time [14]. In previous work, forward momentum is generated by the body pushing against the fluid which requires modeling of the environment and the device body [4-7]. Therefore, the interactions between the flexible material and the environment are critical to understanding the proposed device and such methods were not appropriate. Therefore, a PRB model was used due to its success in approximating undulatory motion in a fluid [15].

In the proposed model, a torsion spring and damper are added to each joint to represent the stiffness and damping of the selected flexible material (see Fig. 1c). The model dynamics are characterized such that each link's inertia comprises the system inertia and the hydrodynamic forces are applied to the center of mass of each link. The number of links selected was determined by balancing the need for fast and accurate computation to use the model for model fitting and optimization; this is discussed

further in the paper. The flexible beam is called the spine and the rigid length element is called the length constraint. The length constraint is applied to the continuum material, such that its natural configuration is in one of two "C" shapes, facing either left or right, highlighting the bistable nature of the system (see Fig. 2b).

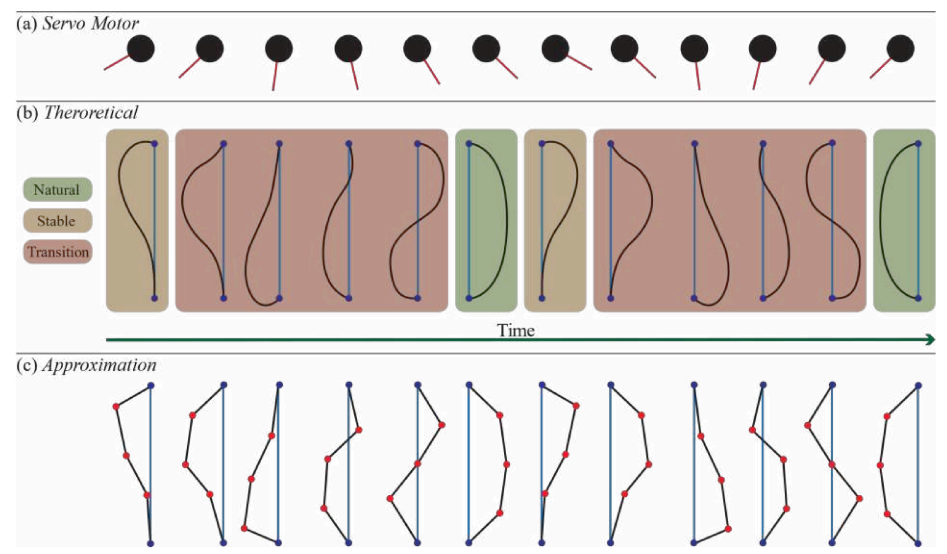


**Fig. 2.** (a) Servo motor control input positions at correlated positions of theoretical and approximated gait. Control input depicts a single period of a sinusoidal waveform that represents a single gait cycle of the device. (b) Theoretical representation of the proposed device in different transition phases between bistable natural states (highlighted green) over time (green arrow). The stable configurations (highlighted orange) are the starting states of the gait cycle and the transition phases (highlighted red) promote wave propagation. The blue lines represent the length constraint that forces the geometric configuration. (c) The approximated representation is a visualization of how we model the phases of the proposed device using PRB. The red dots represent the approximated joints that estimate the material property of the spine.

Our intent is to use this model to analyze the dynamics of the device as it transitions between bi-stable states. Analyzing the two stable states is critical because it is the continuous transition between each that generates the forward thrust of the device (see Fig. 2). The excitation for the device to transition between stable equilibrium depends on the material's internal stiffness characteristics and the length of the geometric constraint. We use the model generated in simulation to understand how the material, beam geometry, and length constraint affects the performance of the device in water. To build the designed model (see Fig. 1), we selected MuJoCo¹ because it has been developed with the intent for model-based optimizations, which was critical for the design process of the mechanism [16].

MuJoCo, DeepMind Technologies Limited. MuJoCo is an open source, full-featured rigid body physics simulator.

#### 2.2 Design Process

Based on assumptions of the physical environment, design decisions need to be made before characterizing the model and manufacturing the prototype. The primary assumption for the system is that the device will operate in water and is constrained to operate within planar motion to match our physical experiment's limited workspace, which is discussed later in this section. Therefore, it is critical that the material selected for the spine has material properties that match this environment. Namely, matching the impedance of the material to the environment is critical in maximizing performance. A composite fiberglass sheet was selected for its low damping and high stiffness to maximize the time spent in transition between stable states since this is responsible for propagating a wave in the spine to generate thrust. These characteristics were critical to ensure the spine was responsive to excitation and to maximize the amount of energy transferred to the environment.

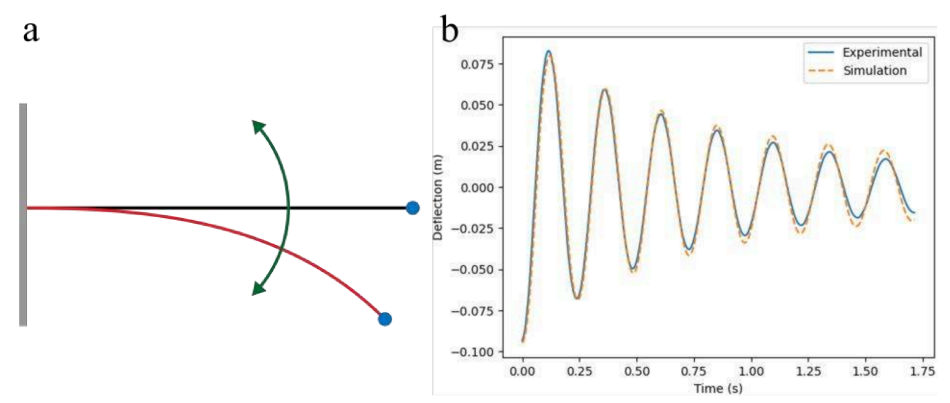


**Fig. 3.** (a) Visualization of beam deflection test where one side of the beam was fixed (gray) and started with an initial deflection (red) and let it come to rest to its natural state (black) with a reflective tracker (blue) to collect tip position information. (b) Results of the simulated and experimental deflection test of the 0.01-inch Fiberglass sheet. The estimated stiffness and damping constants were found using the pseudo rigid body model and optimized joint parameters through Python library, SciPy minimize function.

To model the fiberglass sheet, a deflection test was conducted to parameterize the estimated torsion spring and damping constants for the approximated flexible material. To calculate these values, we conducted a beam deflection experiment, where the tip of a 170x40 mm fiberglass beam was elastically deformed and released, coming then to rest. The tip of the deflected beam was tracked using an OptiTrack motion capture system at 360 fps. An equivalent model was then created in the MuJoCo simulator and the SciPy library<sup>2</sup> was used to fit the simulated tip data to the collected experimental data (see Fig. 3). To prevent the inherent viscoelastic hysteresis of the

A bound-constrained scipy.optimize.minimize() function was used for all optimizations. Implementation was done to minimize a scalar square error through adjusting parameters of the simulation model. Bounds of parameters were selected through physical limitations of the system.

material from dominating model parameters, the experimental data was truncated at the point where the amplitude of the initial displacement attenuates to 80%. For a small displacement, viscoelasticity causes a flexible material to creep over an extended period to reach its final neutral position [17]. The included creep data would reflect a higher estimated damping constant because the material's shift in trajectory reflects energy absorbed over longer time periods. Based on the fitted data, a torsional stiffness and damping constant were found and implemented as joint parameters for the selected fiberglass sheet (see Table 1).

After parameterization of the spine, further optimizations were run to maximize the speed of the actuated system. In dynamics, there is a strong influence of excitation frequency on the system behavior [18]. However, due to the limitations of the actuator, it was not possible to conduct a frequency sweep to find the resonance frequency of the device. Therefore, the frequency of the actuator and the length of the spine were kept constant during the optimization because of the actuator limitations and the size of the experimental tank, respectively. The length of the constrained beam and the amplitude of the input signal were selected to maximize average speed over the simulation time. From those optimizations, the ideal device parameters can be seen in Fig 5.

#### 2.3 Prototype

Table 1. Parameters of Device and Simulation

Parameter	Value
Spine Length	400 mm
Spine Height	40 mm
Material Thickness	0.01 in
Optimized System Energy Loss	0.090685951
Torsional Stiffness Constant (k)	0.8764 N·m/rad
Torsional Damping Constant (C)	4.511·10 <sup>-4</sup> N·m·s/rad
Servo Amplitude	115 degrees
Frequency	0.5 Hz
Material Density	$1235 \text{ kg/m}^3$
Environment Density	$1000 \text{ kg/m}^3$
Environment Viscosity	0.0009 Pa·s

A physical prototype was manufactured based on the simulated model (Fig. 4a). The spine was laser cut from a 0.01-inch Fiberglass sheet using an Epilog Laser Fusion M2; the actuator selected was a Dynamixel (XM430-W210-T); this actuator met the specifications found in Table 1. The actuator specifications were determined through analysis of motor parameters that allowed for wave propagation in the simulated model. The experiment then proceeds as follows. The prototype is controlled using the Dynamixel's onboard closed-loop position controller. A Python script calculates the time-based sinusoidal waveform signal to send the actuator based on a given frequency; this is then transmitted via UART to a Dynamixel OpenCM 9.04 Type-C

Module that connects to the servo (see Fig. 4b). The servo driver then returns the current position and status of the actuator to receive the next command.

#### 2.4 Experimental Setup

To validate the model and design optimization discussed previously, the prototype was run in a water tank to compare against simulated results. The simulation was run under ideal conditions to observe the behavior of the device in water. This meant that buoyancy, hydrodynamic forces generated from turbulence, and environmental factors such as wind were not considered. To minimize discrepancies, the prototype was tested in an enclosed tank (4x2x2 ft) with a low-friction gantry system that permits x and y-axis motion over the surface of the water but restricts motion corresponding to the vehicle's depth (see Fig. 4b). This allowed the device to be suspended in water at a fixed height, to limit the effects of buoyancy.

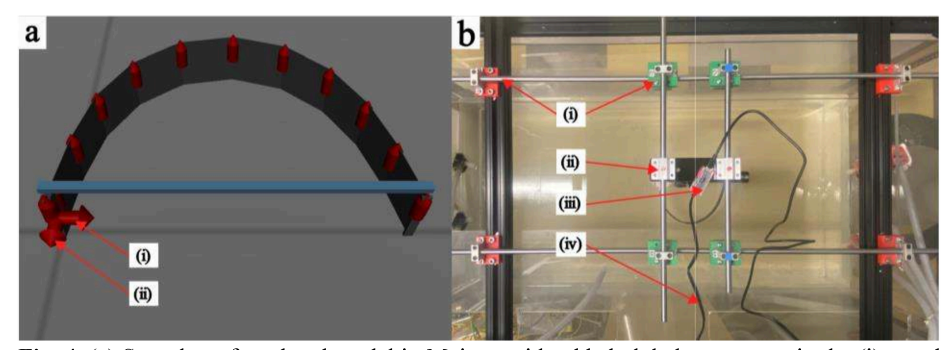


**Fig. 4.** (a) Snapshot of rendered model in Mujoco with added global movement in the (i) x and (ii) y-axis to represent the experimental gantry system. (b) Experimental setup for conducting a planar swimming test. Experimental testing consisted of (i) planar gantry mechanism using low friction linear bearings, (ii) device attachment point with red tracking dots, (iii) onboard Dynamixel OpenCM 9.04 Type-C servo driver transmitting position information to a computer via data-cable, and (iv) power cable to supply 12VDC 1A power to actuator.

To ensure that the model can be validated for real-world applications, data was collected during the experiments. The tests were recorded at 60 frames per second and imported into motion tracking software<sup>3</sup> to interpret position data of the trackers (see Fig. 4b). The positions were collected at the front of the device. Reflections on the water's surface made additional marker placement difficult and therefore visual correlation was used to verify the wave propagation between the simulation and prototype. These results were then validated by the device's average velocities.

<sup>&</sup>lt;sup>3</sup> Tracker: Video Analysis and Modeling Tool

#### 3 Results

To validate the simulation to the prototype, additional post-processing of the data and calibration of the model to the experimental setup was required. To minimize interference of the water tank on the device, the experimental data was truncated. As the prototype reached the end of the tank, the turbulence created from the wave propagation bounced off the walls of the tank and reflected towards the device. This resulted in a portion of the generated thrust to be negated from these disturbances. The experimental data was thus truncated to the initial 4.5 seconds of each test to minimize the differences due to the build-up of wave-based disturbances.

There are several discrepancies in the experimental setup that the simulation does not account for. This includes real-world wall effects observed due to the tank size and material property nonlinearities, as well as friction and inertial effects observed in the gantry system (see Fig 4b). Therefore, the simulation was calibrated to consolidate discrepancies observed in the experiments. By tuning the x and y-axis friction constants of the simulated gantry system, the model speed was fitted to the average velocity across multiple length-constraint experimental tests (see Fig. 4a). The calibration was conducted by fitting the simulation average velocity to the experimental velocities at each length constraint. The average friction coefficient across all the length constraints was then used as the calibrated energy loss seen in the real-world system (see Table 1). The calibrated simulation compared to the experimental data can be seen in Fig 5b. The differences in the calibrated model and prototype are likely due to the simplified hydrodynamic model. The benefits and tradeoffs of this approach are further discussed in the conclusions section of this paper.

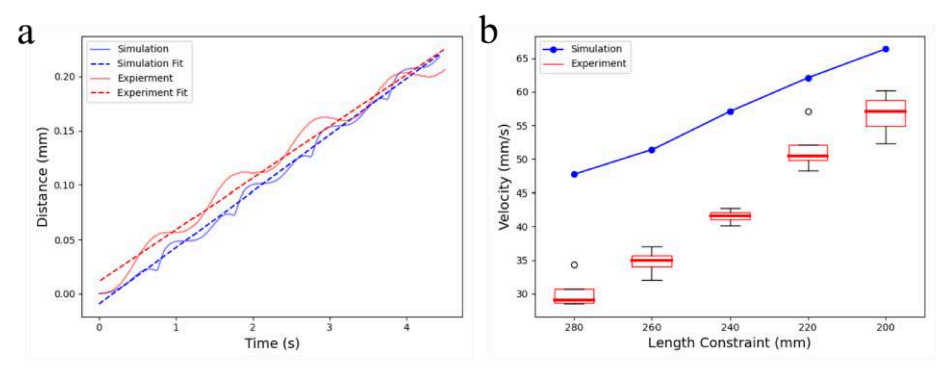


**Fig. 5.** (a) Example plot of position (in the direction of motion) versus time for calibrated simulated model (blue) and experimental prototype (red). The simulation was calculated at the same parameters for the respective experiment. In this plot the length constraint was 220 mm, and the signal input amplitude was 115°. Both data sets were then fitted to a linear regression model (dashed lines) to approximate the average speed of the device. (b) Trend of calibrated simulation (blue) and device speeds (red) as a function of different length constraints. For each length constraint, the experiment was run four times, and an average velocity (red line) was calculated using linear regression. The box plots are defined such that the horizontal line represents the median and the box bounds are the upper and lower quartiles. Outliers in the data set are represented as circles.

Despite the discrepancy in overall device speed, the model can accurately suggest correlations between parameters and outputs. Multiple tests over a range of length constraints were conducted to validate the model for the physical device. As seen in Fig 5b, shortening the length constraints in both simulation and experiments correlates to a higher average device speed. Additionally, the model was configured for maximum velocity with a length constraint of 200 mm and input signal amplitude of 80° was determined as the minimum to initiate bistable transitions. This is reflected in the average speeds from the tests conducted at this length constraint (see Fig 5b). However, the amplitude value discovered in simulation did not successfully initiate a transition between stable states in the prototype. A higher amplitude was thus needed to generate successful wave propagation in the prototype. This is most likely due to differences between the PRB model and the real behavior of the fiberglass sheet. To accurately compare the simulations and experiments, the input signal amplitude was matched to the experimentally used input signal. Overall, there is a qualitative similarity between the model and device that suggests that the simulation results provide evidence towards a validated prototype.

From the experiments with the prototype, it was observed that material selection in relation to the working environment is critical. In the case of water, a softer material is necessary to slow down wave propagation in our prototype to allow for the spine to transition between stable states. If a stiffer material or shorter spine is used, this results in faster snapping and less-effective thrust generation. This implies that the continuous transition between stable states is critical and minimizing the time spent in the natural configuration of the device produces more continuous thrust. This can be seen in the oscillatory behavior visible in Fig. 5a. The discrepancies between simulation and experimental oscillations can be attributed to the model discrepancies discussed above.

### 4 Conclusion

In this paper, we modeled and characterized a compliant bistable undulatory robot. An analytical model was generated using geometric approximation of the compliant material to parameterize the variables critical to wave propagation and thrust generation. We selected and experimentally identified the material properties of a fiberglass sheet to estimate the stiffness and damping of a hinge joint with a damper and torsion spring. A prototype of the device was manufactured, and experiments were conducted to validate the simulated model at various length constraints. While there were clear differences in velocity between the simulations and tests, the model and prototype both showed similar performance trends across a range of length constraints. The discrepancies between the model and device can be attributed to the real-world mechanical constraints and known simplifications of the model, which at this point still requires real-world testing to properly calibrate. We believe that adding computational fluid dynamics to the model would help address some of the issues observed, albeit at a higher computational cost.

Future work will investigate how the constrained beam model can be optimized for various materials and environments to explore the tunability of material selection and actuator control for the device. This will include design variations that connect multiple length-constrained units to further explore hybrid, compliant swimming fins. Additionally, future work will include attaching a buoyancy mechanism so that the device floats on the surface of the fluid so that free swimming experiments can be conducted. Furthermore, using a higher fidelity fluidic model would allow for analysis on the device's resonance frequency which would allow for increased efficiency of device. By taking advantage of continuum materials, it is possible to lower manufacturing time of soft robots and allows for high adaptability for these devices. This paper aims to present preliminary work within the field of soft robotics on exploring low cost, bistable systems that can be modeled via a simplified physics-based approach.

**Funding.** This work is supported by the National Science Foundation (NSF) Grant No. 1935324.

#### References

- 1. M. J. Lighthill, "Aquatic animal propulsion of high hydromechanical efficiency," *Journal of Fluid Mechanics*, vol. 44, no. 02, p. 265, 1970.
- 2. G. V. Lauder and E. D. Tytell, "Hydrodynamics of undulatory propulsion," *Fish Physiology*, pp. 425–468, 2005.
- 3. E. D. Tytell and G. V. Lauder, "The hydrodynamics of Eel Swimming," *Journal of Experimental Biology*, vol. 207, no. 11, pp. 1825–1841, 2004.
- 4. H. Feng, Y. Sun, P. A. Todd, and H. P. Lee, "Body wave generation for anguilliform locomotion using a fiber-reinforced soft fluidic elastomer actuator array toward the development of the EEL-inspired underwater soft robot," *Soft Robotics*, vol. 7, no. 2, pp. 233–250, 2020.
- 5. D. Q. Nguyen and V. A. Ho, "Kinematic evaluation of a series of soft actuators in designing an eel-inspired robot," 2020 IEEE/SICE International Symposium on System Integration (SII), pp. 1288–1293, Jan. 2020.
- M. Fremerey, L. Fischheiter, J. Mämpel, and H. Witte, "Locomotion Study of a single actuated, Modular Swimming Robot," WIT Transactions on Ecology and the Environment, 2010.
- 7. Chen, Z. Wu, H. Dong, M. Tan, and J. Yu, "Exploration of swimming performance for a biomimetic multi-joint robotic fish with a compliant passive joint," *Bioinspiration & Biomimetics*, vol. 16, no. 2, p. 026007, 2020.
- 8. Y. Xu, J. Hu, J. Song, F. Xie, Q. Zuo, and K. He, "A novel multiple synchronous compliant and passive propeller inspired by loons for Swimming Robot," 2022 IEEE International Conference on Robotics and Biomimetics (ROBIO), 2022.
- 9. M. Sharifzadeh, Y. Jiang, and D. M. Aukes, "Reconfigurable curved beams for selectable swimming gaits in an underwater robot," *IEEE Robotics and Automation Letters*, vol. 6, no. 2, pp. 3437–3444, 2021.
- 10. M. Sharifzadeh and D. M. Aukes, "Curvature-induced buckling for flapping-wing vehicles," *IEEE/ASME Transactions on Mechatronics*, vol. 26, no. 1, pp. 503–514, 2021.

- Y. Jiang, M. Sharifzadeh, and D. M. Aukes, "Shape change propagation through soft curved materials for dynamically-tuned paddling robots," 2021 IEEE 4th International Conference on Soft Robotics (RoboSoft), 2021.
- 12. Y. Jiang, F. Chen and D. M. Aukes, "Tunable Dynamic Walking via Soft Twisted Beam Vibration," in IEEE Robotics and Automation Letters, vol. 8, no. 4, pp. 1967-1974, April 2023, <a href="https://doi.org/10.1109/LRA.2023.3244716">https://doi.org/10.1109/LRA.2023.3244716</a>.
- T. D. Ta, T. Umedachi, and Y. Kawahara, "A multigait stringy robot with bi-stable soft-bodied structures in multiple viscous environments," 2020 IEEE/RSJ International Conference on Intelligent Robots and Systems (IROS), 2020. doi:10.1109/iros45743.2020.9341059
- 14. Bijian Chen and M. Govindaraj, "A physically based model of fabric drape using flexible shell theory," *Textile Research Journal*, vol. 65, no. 6, pp. 324–330, 1995.
- 15. K. A. Melsaac and J. P. Ostrowski, "A geometric approach to anguilliform locomotion: Modeling of an underwater Eel Robot," *Proceedings 1999 IEEE International Conference on Robotics and Automation (Cat. No.99CH36288C)*.
- E. Todorov, T. Erez, and Y. Tassa, "MuJoCo: A physics engine for model-based control," in *IEEE/RSJ International Conference on Intelligent Robots and Systems (IROS)*, 2012, pp. 5026–5033
- 17. S. Mei and Y. Wang, "Viscoelasticity: A new perspective on correlation between concrete creep and damping," *Construction and Building Materials*, vol. 265, p. 120557, 2020.
- X. Wang and S. Alben, "Dynamics and locomotion of flexible foils in a frictional environment," *Proceedings of the Royal Society A: Mathematical, Physical and Engineering Sciences*, vol. 474, no. 2209, p. 20170503, 2018. doi:10.1098/rspa.2017.0503